PASJ: Publ. Astron. Soc. Japan **45**, 139–151 (1993)

CO Observations of Edge-on Galaxies. III. NGC 891: Threshold Radius for a Star-Formation Disk

Yoshiaki SOFUE
Institute of Astronomy, The University of Tokyo, Mitaka, Tokyo 181
and
Naomasa NAKAI
Nobeyama Radio Observatory, Minamimaki-mura, Minamisaku-gun, Nagano 384-13*

(Received 1992 June 2; accepted 1992 September 21)

Abstract

Edge-on galaxy NGC 891 has been observed in ^{12}CO(J = 1–0)-line emission using the Nobeyama 45-m telescope at an angular resolution of 15″. We obtained an intensity distribution and a position-velocity diagram along the major axis for a length of ±5′ about the galaxy center. We derived the radial distributions of the molecular gas density and surface mass density. The results indicate the presence of (a) a molecular gas ring of 3.5 kpc radius associated with an extended outer disk having a flat rotation, (b) a rigidly-rotating inner disk or a bar of radius of 3 kpc, and (c) a compact nuclear component showing a rigid rotation and high-velocity dispersion. From the molecular ring structure and kinematical characteristics, we conclude that NGC 891 is an SBb galaxy. The molecular gas within the bar part is shown to be rotating rigidly. We find that there exists a threshold radius for the star-formation rate in the gas disk: The star-formation efficiency is almost constant within 2′.2 (= 5.7 kpc; threshold radius), while it decreases steeply beyond this radius. This implies that the star-formation rate is not uniquely determined by the gas density, but is also strongly dependent on the structural conditions within the galaxy disk. We obtained a map toward the tangential direction of the molecular ring within the main disk, which indicates the presence of a molecular gas spur extending for a few scale heights of the disk. The map also shows the existence of an extended molecular gas disk of 2 kpc thickness, which comprises about 35% of the total molecular mass.

Key words: CO emission — Galaxies: edge-on — Molecular hydrogen — Rotation curve — Stars: formation

1. Introduction

The molecular gas distribution and its kinematics of spiral galaxy NGC 891 have been observed extensively in CO line emission (Solomon 1983; Sofue et al. 1987; García-Burillo et al. 1992). An almost perfect edge-on galaxy like NGC 891 provides a unique opportunity to investigate the rotation characteristics and global radial distribution of gas in the disk. It should be stressed that even one-dimensional scans along the major axis provide fairly complete information about these; this is particularly effective for single-dish, high-resolution observations of molecular lines at mm wavelengths.

Another important aspect of observing edge-on galaxies is to study the vertical extent and distribution both in emission (e.g., Aoki et al. 1991), and in absorption by molecular gas in halos often observed as optical dark lanes emerging from the disk planes (see, e.g., Sandage 1961; Sawa and Fujimoto 1987; Sofue 1987; Handa et al. 1992). Recently, a thick disk of molecular gas in NGC 891 was detected in CO by García-Burillo et al. (1992).

In this context, we conducted a systematic CO line survey of edge-on galaxies using the 45-m telescope of the Nobeyama Radio Observatory at an angular resolution of 15″ [Sofue et al. 1987 (Paper I); Sofue et al. 1989 (Paper II)]. This paper is the third of a series presenting the results, and reports an almost complete CO line survey along the major axis of NGC 891.

NGC 891 has also been observed extensively at various radio wavelengths both in continuum and H I line emission at a comparable angular resolution (e.g., Sancisi and Allen 1978; Rupen 1990).

We compare our results from the CO line observations with those radio data at various wavelengths and discuss the star-formation efficiency within the disk.

* Nobeyama Radio Observatory (NRO) is a branch of the National Astronomical Observatory, an inter-university research institute operated by the Ministry of Education, Science and Culture.

Table 1. Parameters for NGC 891.

The center reference position ($X = 0''$, $Y = 0''$)*	
R.A.$_{1950}$	$02^h19^m24^s.3$
Decl.$_{1950}$	$42°07'17''.0$
V_{LSR}	525 km s^{-1}
Distance†	8.9 Mpc
Position angle of the major axis	23°.0
Inclination angle‡	> 88°.3

* Sancisi and Allen (1979). † Handa et al. (1992). ‡ Measured from the CO disk thickness.

2. Observations

Observations of the ^{12}CO(J = 1–0) line of NGC 891 were made from 1992 January 8 to 17, using the 45-m telescope of the Nobeyama Radio Observatory as a part of the survey of edge-on galaxies. The parameters for the galaxy are listed in table 1. Here, we adopt a distance of 8.9 Mpc of the galaxy, which was derived from a Tully-Fisher relation applied to an H-band magnitude and an H I line width (Handa et al. 1992). Hence, the linear scale at the galaxy corresponds to $1' = 2.59$ kpc. Note that our earlier results (Sofue et al. 1987) were based on a distance of 14 Mpc. The LSR systemic velocity of the galaxy is assumed to be $V_{sys} = 525$ km s^{-1}.

The antenna had an HPBW of 15″ (= 647 pc) at 115.271 GHz, and aperture and main-beam efficiencies of $\eta_a = 0.35$ and $\eta_{mb} = 0.50$, respectively. We used an SIS receiver combined with a 2048-channel acousto-optical spectrometer of 250 MHz bandwidth corresponding to a velocity coverage of 650 km s^{-1}. After binding up every 32 channels in order to increase the signal-to-noise ratio, we obtained spectra with a velocity resolution of 10.2 km s^{-1}. The system noise temperatue (SSB) was 600 to 800 K at the observing elevations (40° to 80°). The calibration of the line intensity was made using an absorbing chopper in front of the receiver, yielding an antenna temperature (T_A^*), corrected for both atmospheric and antenna ohmic losses.

We used a multi-on-off switching mode, with which we observed six positions and two off positions at ±5′ east and west in a single sequence of observing runs. In each run we observed the center for a reference in order to check the pointing and intensity calibration. Hence the center was observed many times. The grid spacing was taken to be 15″. The on-source total integration time was about 5 to 10 min per each point, while the center was observed repeatedly to obtain an integration time of 1.5 hr. The rms noise of the resultant spectra at velocity resolution of 10 km s^{-1} was typically 20 mK in T_A^* for the disk region. The pointing of the antenna was made by observing nearby SiO maser sources at 43 GHz every 1 to 1.5 hr.

3. Results

3.1. *Spectra*

The obtained CO spectra at a velocity resolution of 10 km s^{-1} are shown in figure 1a. The intensity scale used in this paper is the main-beam brightness temperature [T_{mb} ($\equiv T_A^*/\eta_{mb}$)], and the LSR radial velocity (V_{LSR}) was used. We used a right-hand coordinates system, X and Y, based on the distances along the major and minor axes from the center position, respectively: X is positive toward the north-east (N) at a position angle of 23°.0, and Y is positive toward the north-west perpendicular to the X-axis. CO emission was detected at all positions along the major axis from $X = -4'.5$ (11.7 kpc) to $+5'$ (13 kpc). The emission profiles of temperatures as high as $T_{mb} \sim 0.7$–1.1 K were observed at $|X| < 2'$. The spectra clearly show the galactic rotation: blueshifted at positive X, and redshifted at negative X.

The spectrum toward the center is enlarged and shown in the inset in figure 1b, which was obtained by averaging the results from all of the observing runs. The spectrum shows a narrow, bright component with a peak temperature of $T_{mb} = 1.1$ K and a velocity width of about 70 km s^{-1} at the systemic velocity. The spectrum is superposed by an extended, broad component with a very high velocity dispersion with a width as large as 600 km s^{-1}. The integrated intensity toward the center is 130 K km s^{-1}. CO emission as high as $T_{mb} \sim 0.8$ K was observed toward the outer disk regions at $X \sim \pm 1'$–$2'$. Some spectra (e.g., at $X = 1'$–$1'.5$) show double or more peaks, which are naturally interpreted as being due to multiple spiral arms separated in radial velocities.

3.2. *Total Velocity Profile*

By averaging the spectra along the major axis, we obtained a "total" velocity profile (figure 2). Profile shows a typical double-peaked emission, characteristic of a rotating ring; the majority of the emission comes from the flat-rotation part of the disk. The double peaks appear at ±200 km s^{-1} with respect to the systemic velocity of $V_{LSR} = 525$ km s^{-1}; the 20%-level velocity width

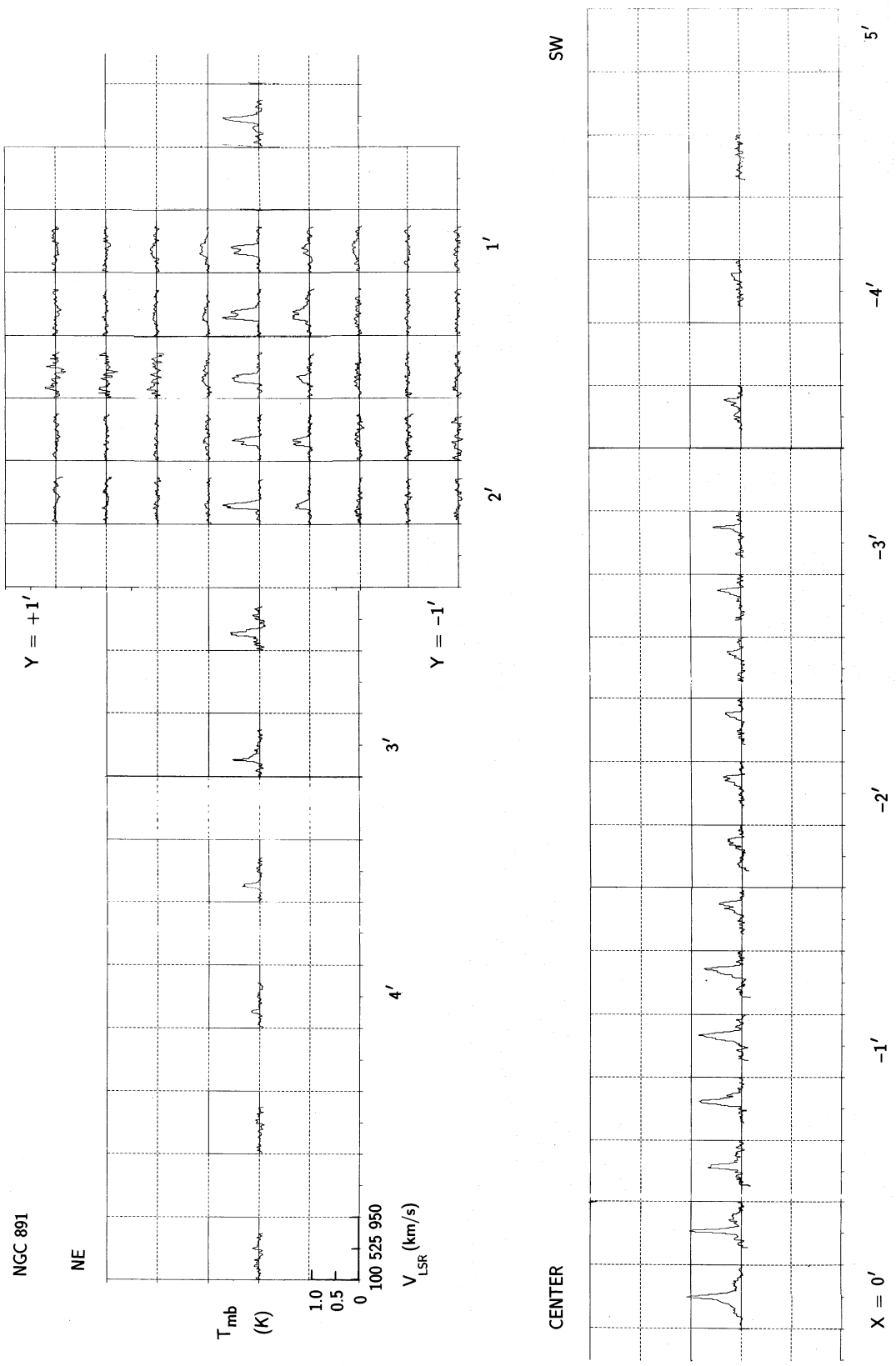

Fig. 1a. Observed I_{CO} line profiles of NGC 891 with a velocity resolution of $\Delta V = 10$ km s^{-1}.

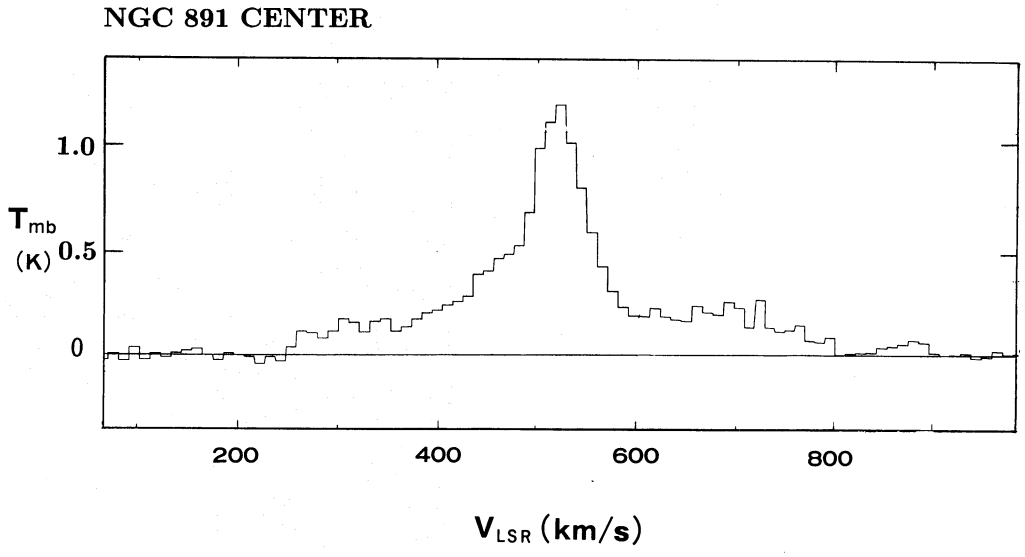

Fig. 1b. The spectrum toward the center.

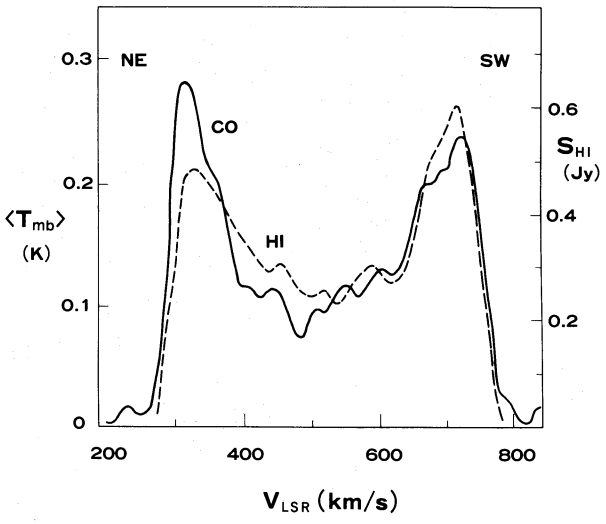

Fig. 2. Total line profiles of the ^{12}CO($J = 1$–0) emission (full line). The H I total line profile (Sancisi and Allen 1979) is shown by the dashed line.

of this profile is 490 km s^{-1}. This width is in coincidence with that observed in the H I emission, 478 to 490 km s^{-1} (Huchtmeier and Richter 1989). It is interesting to compare the total CO profile with the total H I profile, which is indicated by the dashed line, as reproduced from Sancisi and Allen (1979) (see also Rupen 1990). We find a striking coincidence between the H I and CO line profiles, particularly their velocity widths and double-horn structures. We note even larger velocity CO outskirts at ±300 km s^{-1}, which result from the central broad velocity component. However, these outskirts are far weaker compared to the double-horn parts, and do not significantly contribute the line-width measurement. These facts indicate that the CO line width is a promising tool for a Tully-Fisher (1977) relation for galaxies at distances greater than about 100 Mpc, beyond which H I measurement becomes even more difficlut than measuring the CO line widths (Dickey and Kazes 1992; Sofue 1992).

Although the H I and CO profiles of NGC 891 generally coincide with each other, there is difference between the north-south assymmetries in the total profiles: In CO, the northern part is stronger and, therefore, indicates more molecular gas than the southern part.

On the other hand, the H I profile shows an asymmetry of the opposite sense: The southern H I emission is stronger and, therefore, the CO and H I intensities seem to be anti-correlated with each other. Such an anti-correlation could be related to an N-S asymmetry under the condition for the presence of a gaseous state, either in atomic or molecular, and might be related to an interstellar conversion process from H I to molecules, or vice versa.

3.3. Intensity Distribution

The distribution of the integrated line intensity I_{CO} [$= \int T_{mb}\, dV$ (K km s^{-1})] is plotted against X in figure 3. The intensity has a maximum as strong as $I_{CO} =$ 130 K km s^{-1} toward the galaxy center. This central peak is a contribution from the nuclear region with broad

emission profile. The spatial extent of this component is as sharp as 30″ in diameter and is slightly shifted toward the SW.

The I_{CO} distribution indicates two more major peaks at $X = 1'.2$ and at $-1'$. These may indicate the existence of a ring-like concentration of gas at a radius of about 3.5 kpc from the center, which we hereafter call the "3.5-kpc molecular ring," although they could be alternatively interpreted as being due to tangential views of symmetrical spiral arms. This 3.5-kpc ring is then followed by a more extended intensity distribution, which is visible until $X \sim \pm 4'.5$ (11.7 kpc), while no significant molecular gas is detected beyond the radius 11.7 kpc. Beyond the 3.5-kpc ring, several peaks are visible in figure 3a; these may be due either to spiral arms or additional ring structures in the disk. We note that the present result confirms our earlier result (Sofue et al. 1987) within the errors.

The dashed line in figure 3a indicates the distribution of the 6-cm continuum emission at an angular resolution 20″ plotted against X, as obtained from the data of Sukumar and Allen (1991). The three major CO peaks at $X = 0', 1'.2$, and $-1'$ coincide exactly with the radio continuum peaks at 6 cm. The CO emission is better correlated with 6-cm emission than the 21-cm continuum (Sancisi and Allen 1979). We also point out that the CO and 6-cm peaks coincide with the regions of depolarization of the linearly polarized emission (Sukumar and Allen 1991). These facts may be a natural consequence of the correlation between star-formation activity within the disk and the molecular gas concentration. On the other hand, the H I emission (Sancisi and Allen 1979) is visible outside the molecular ring, having maxima at 2′–3′. Moreover, the H I emission shows a depression toward the center (see figures 3b and c).

3.4. *Radial Distribution*

Deriving the radial distribution of molecular gas from the intensity distribution is not straightforward. As is shown in subsections 3.6 and 3.7, the rotation curve of the galaxy is almost flat from the very inner region to the outer disk. Using this fact, we can obtain the distribution of the flat-rotating gas. Namely, we obtained I_{CO} by integrating the CO line profiles for a certain velocity range around the terminal velocities, $V_{min} < |V_{LSR} - V_{sys}| < V_{max}$ km s^{-1}. The intensity can then be converted to the column density of H_2, which is indicated by the solid lines in figure 3b separately for the NE and SW sides. Here, V_{min} and V_{max} are the minimum and maximum velocities of integration with respect to the systemic velocity. We chose here $V_{min} = 197$ km s^{-1} and $V_{max} = 257$ km s^{-1} in order to compare the result with those obtained by Rupen (1990) for the H I line emission by using their intensity maps for the edge-most channels. The distribution of the H I column density is also shown in figure 3b.

If the gas is rotating circularly at an almost constant velocity of V_{rot}, the above velocity range corresponds to the line-of-sight depth of integrated gas (l) through

$$l = 2|X|\sqrt{V_{rot}^2/V_{min}^2 - 1}. \quad (1)$$

For $V_{min} = 197$ km s^{-1} and V_{rot}=230 km s^{-1}, we have $l = 1.21|X|$.

Figure 3b shows an NE-SW averaged column density (in H atoms cm^{-2}) obtained from the integrated intensity for the same velocity range as a function of the distance from the galactic center. In the figure we also plot the column density of the H I gas [N(H I) (in H atoms cm^{-2})], which was derived from the H I intensity distribution for the same velocity range, using the data presented by Rupen (1990).

The surface mass density of the molecular gas [$S(R = |X|)$] can be obtained approximately by

$$S_{H_2} = CI_{CO}b_{CO}/l, \quad (2)$$

and

$$S_{H\ I} = N(\text{H I})b_{H\ I}/l, \quad (3)$$

where b_{CO} and $b_{H\ I}$ are the beam widths of the CO and H I observations (15″=647 pc for CO; 20″=863 pc for H I) in the same units as for l; C is the conversion factor from the CO intensity to the H_2 column density.

Figure 3c shows the radial distributions of the surface mass densities [S (in $M_\odot$ pc^{-2})] for the molecular and atomic hydrogen gases, as derived by using figure 3b. Here, we can see more clearly the 3.5-kpc ring of the molecular gas, as well as the central concentration. On the other hand, the H I gas is almost absent near the galactic center, but shows a broad ring-like distribution having a largely extended outskirt. Note that the H I thickness of the disk is slightly larger than the beam width of the observation (Rupen 1990); the true surface density should thus be larger than the value given in figure 3c.

The approximate density of gas at radius X [n ($R = |X|$)] can be obtained by dividing I_{CO} by l: $n_{H_2} = S/b = CI_{CO}/l$. Note that the thus-obtained density is an "beam-diluted" density, averaged in the direction perpendicular to the galactic plane by the beam width. Therefore, if the thickness of the gas layer is t, the "true" spatial density can be derived by multiplying by a factor of b/t. If we assume a disk thickness of $t \simeq 100$ pc, the spatial density can be obtained by multiplying by a factor of 647 pc/100 pc = 6.47 to n_{H_2}.

3.5. *The Molecular Mass*

Since we can safely assume that the beam width (15″=647 pc) is sufficiently larger than the disk thickness and that the observed area covers a sufficiently wide

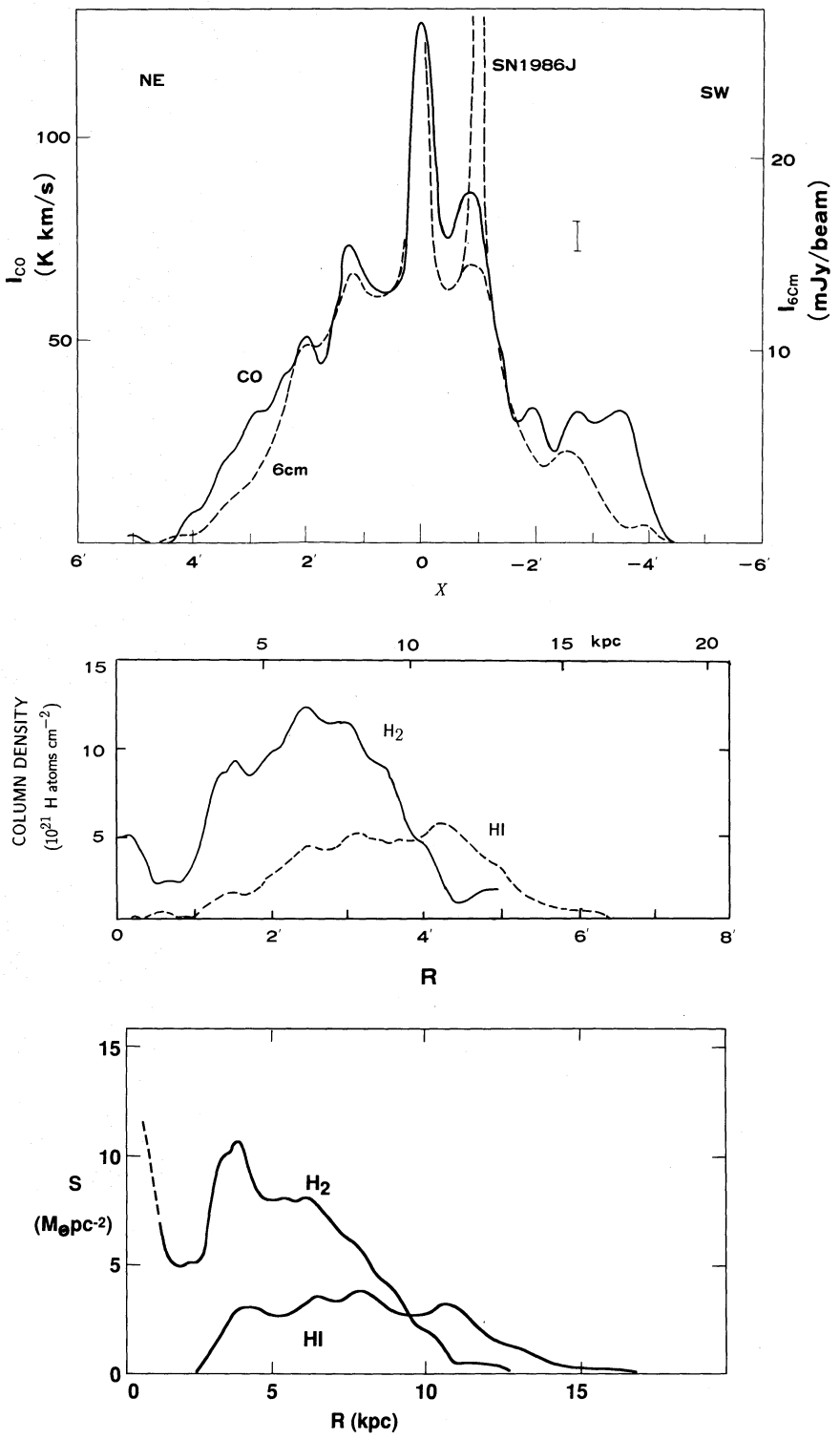

Fig. 3. (a) I_{CO} distribution along the major axis X (full line), and that of the 6-cm continuum intensity, as reproduced from Sukumar and Allen (1991; dashed line). The strong radio intensity peak at $X = -1'$ is a supernova SN 1986J. The vertical bar indicates the typical rms error. (b) Solid line: Column density of H_2 gas (in H atoms cm^{-2}) for a flat rotation disk, obtained by integrating the CO emission within the velocity range of $197 < |V_{LSR} - V_{sys}| < 257$ km s^{-1}. Dashed line: The same for the H I gas, obtained from data by Rupen (1991). (c) Radial distributions of the surface mass densities of H_2 and H I gases.

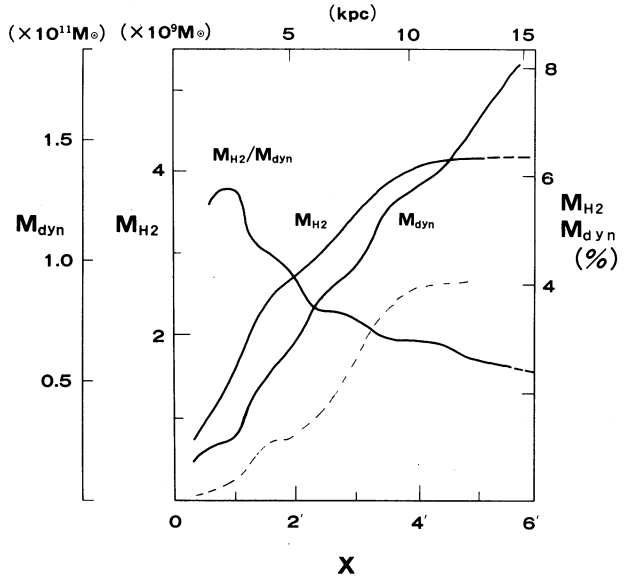

Fig. 4. Molecular gas mass contained in $|X|$; dynamical mass; and the ratio of the molecular mass to the dynamical mass cotained within a radius $R = |X|$. The dashed line shows the molecular gas mass calculated from the radial density distribution in figure 3c.

range along the major axis until the CO emission tends almost to zero, we can estimate the total luminosity of the CO emission and derive the total mass of molecular gas from the data in figure 3a. The total luminosity is estimated to be $L_{\rm CO} = 6.61 \times 10^8$ K km s^{-1} pc^2 for a 8.9 Mpc distance. For a normal conversion factor adopted for molecular clouds, $N({\rm H_2})({\rm cm^{-2}}) = 3.6 \times 10^{20} I_{\rm CO}$ (K km s^{-1}) (Sanders et al. 1984), we obtain the total mass of molecular gas contained in the disk within $\pm 5'$ (13 kpc) to be $3.80 \times 10^9 M_\odot$. We stress that this value is comparable with that of our Galaxy ($3.5 \times 10^9 M_\odot$; Sanders et al. 1984). This value can be compared with our previous estimation (Sofue et al. 1987), which gave 6×10^9 $M_\odot$ for a 14-Mpc distance, or $2.4 \times 10^9 M_\odot$ for a 8.9-Mpc distance. {We comment that, if we adopt the more recent conversion factor from CO to H_2 of 2.8×10^{20} [H_2 cm^{-2}/K km s^{-1}] (Bloemen et al. 1986), the molecular mass should be reduced by a factor of 2.8/3.6=0.778.} We stress here that almost no CO emission is observed beyond 12 kpc, and, hence, the above estimated mass is approximately the total molecular mass of the galaxy.

This molecular mass can be compared with the total dynamical mass of the galaxy. Here, we estimate the dynamical mass by the simple relation $M_{\rm dyn} = RV_{\rm rot}/G$, where G is the gravitational constant. For a rotation velocity of 230 km s^{-1} (see figure 6), we obtain a dynamical mass of $1.43 \times 10^{11} M_\odot$ within 12 kpc. This means that a fraction of 2.5% of the total (dynamical) mass is taken by the molecular gas at this scale. In figure 4 we plot the molecular gas mass and the ratio of the molecular mass to the dynamical mass contained within a radius $R = |X|$. Obviously the molecular gas fraction increases toward the inner region, and, within 2.5 kpc from the nucleus, a fraction larger than 6% of the total mass is taken by hydrogen molecules.

The H_2 mass distribution for the flat-rotation disk can be calculated using the radial distribution of the H_2 density as shown in figure 3c. It is interesting to compare the thus-calculated H_2 mass distribution with that given in figure 4. The H_2 mass of the flat-rotation disk (f.r.d.) within radius R is estimated as $M_{\rm f.r.d.}(R) = 2\pi m_{\rm H} \int_0^R S(r) r dr$. Using the density distribution in figure 3c, we obtain $M_{\rm f.r.d.}(R)$, as shown by the dashed line in figure 4: We have $M_{\rm f.r.d.}(R) = 1.1 \times 10^8$, 7.5×10^8, and $2.5 \times 10^9 M_\odot$, respectively, at R =2.5, 5, and 10 kpc. These should be compared with integrated molecular mass of 1.5, 2.5 and $4 \times 10^9 M_\odot$, respectively, at the corresponding radii. A discrepancy of about $1.5 \times 10^9 M_\odot$ between the mass of the flat-rotating disk and the integrated mass of the molecular gas occurs at $R < 3$–4 kpc, while the integrated mass beyond 4 kpc becomes almost equal to that calculated from the curve in figure 3c. This fact implies that the assumption of flat rotation is not valid for the gas within $R \sim 4$ kpc. In fact, as seen from the position-velocity diagram (figure 5), a significant amount of gas within $R < 3$–4 kpc shows rigid rotation.

3.6. *Position-Velocity Diagram*

Using the spectra along the major axis, we obtained a position-velocity ($X - V$) diagram, which is shown in figures 5a and b in the form of a contour plot and a gray-scale representation, respectively. We find a good coincidence of the present result with the position-velocity diagram obtained with the IRAM 30-m telescope by García-Burillo et al. (1992).

The central region indicates a rigidly rotating disk of radius $\sim 1'$ (2.6 kpc), which appears as the bright ridge traced by the highest to fifth-highest contours around the center in figure 5a. This feature is rotating at its maximum velocity of about 100 to 150 km s^{-1}. This feature is then merged by an outer rigid rotation feature at $|X| > 1'$ with a larger velocity, particularly in the SW part of the galaxy.

We then notice a diffuse, high-velocity dispersion feature near the velocity axis, which is strongly elongated in the velocity direction. This feature is definitely tilted from the velocity axis: It has a positive velocity at $X < 0$, and a negative velocity at $X > 0$. This is simply interpreted as being due to a disk or ring of radius $15''$ (650 pc) which is rapidly rotating at a velocity as high

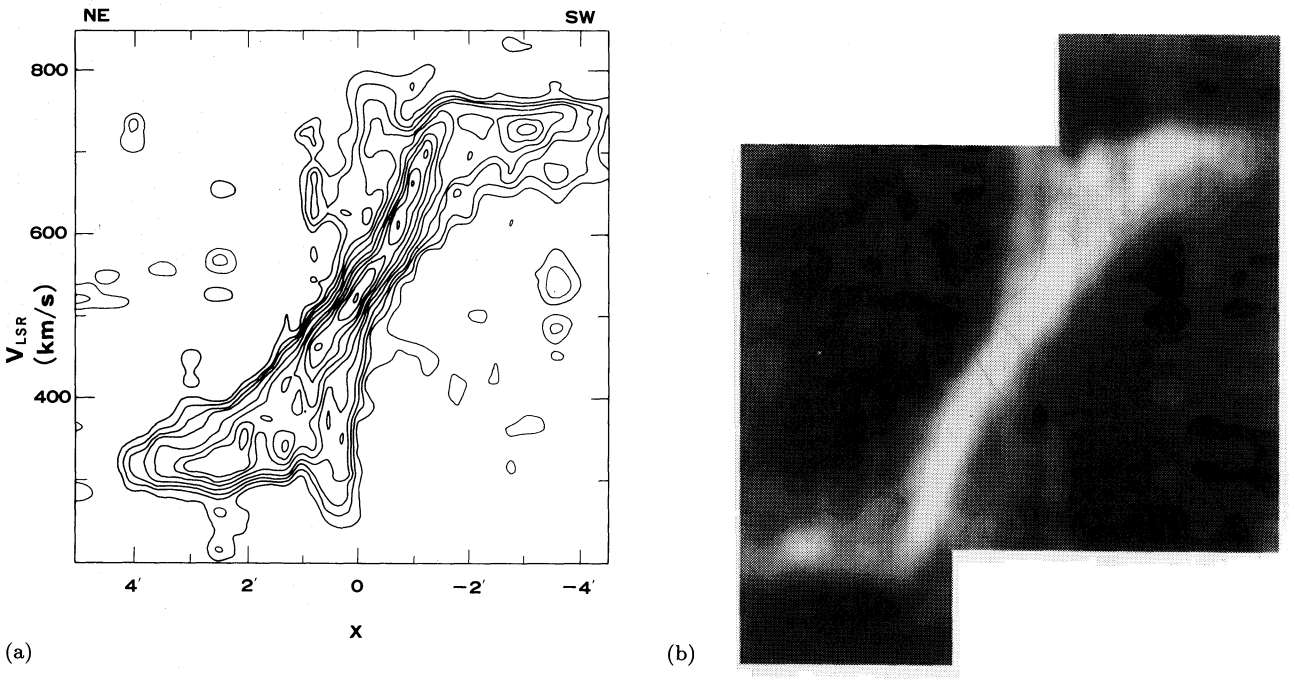

Fig. 5. (a) Position-velocity ($X - V$) diagram along the major axis in contour form. Contours are drawn at T_{mb}= 0.05, 0.10, 0.15, 0.2, 0.3, 0.4, 0.5, 0.6, 0.7, 0.8, 0.9, 1.0 K. (b) The same as (a), but in a gray-scale representation.

as 260 km s^{-1}. Moreover, its rather broad extent in the X direction suggests that the feature is not a simple rotating disk or ring, but that some expansion and/or contraction motion is superimposed on the rotation. This feature, as well as the central dense component, resembles that seen in the longitude-velocity diagram of our Galaxy (e.g., Dame et al. 1987).

In the outer disk beyond $X \sim \pm 1'$, where we observe a main disk comprising the 3.5-kpc molecular ring and its outskirts, the diagram shows an almost flat rotation at $V_{rot} = 230$ km s^{-1}. Some arm-like features are visible in the gray-scale diagram (figure 5b).

As discussed in section 3.5, the molecular mass of the flat-rotation disk, as derived from figure 3c, is not sufficient to explain the total integrated mass; the discrepancy occurs mainly by the region showing the rigid-rotation feature in figure 5. In fact, the rigid-rotation feature within 1.′3 (3.5 kpc) involves a significant amount of gas, which approximately coincides with the amount of discrepancy between the flat-rotation disk and the integrated mass ($1.5 \times 10^9 M_\odot$). In other words, the rigid-rotation feature in figure 5 cannot be reproduced by a circular ring along a radius of 3–4 kpc rotating at the same velocity as the flat-rotation disk, but requires rigidly rotating gas inside 3.5 kpc. Such rigid-rotation gas could be related to a bar structure, as discussed later.

3.7. Rotation Curve

Using the position-velocity map in figure 5, we obtained a rotation curve. First, an apparent terminal velocity is defined by a velocity represented by the lowest contour at each X (V_{term}), which was read from figure 5a by adopting a systemic velocity of $V_{sys} = 525$ km s^{-1}. Then, a contribution from an assumed velocity dispersion of the molecular gas ($\sigma_{gas} = 10$ km s^{-1}) and the velocity resolution of the diagram ($\Delta V = 10$ km s^{-1}), was estimated by $\sigma = (\sigma_{gas}^2 + \Delta V^2)^{1/2} = 14$ km s^{-1}. Finally, σ was reduced from the apparent terminal velocity to obtain the rotation velocity ($V_{rot} = V_{term} - \sigma$) and the northern and southern values were averaged. Figure 6 thus plots the obtained rotation curve.

The CO rotation curve comprises of a steeply increasing part near to the nucleus, attaining a high-velocity rotation of 260 km s^{-1} and decreasing at $R = 30'' - 1'$, and then a flat part of about 230 km s^{-1} beyond 1′. The present rotation curve can be combined with the H I rotation curve (Sancisi and Allen 1979), which is reproduced in figure 6 by the dashed line. The entire diagram indicates a flat rotation characteristic for a wide range of radii [from $R = 1'$ (2.6 kpc) to 6′ (15.5 kpc)], beyond which it gradually decreases until 9′ (23 kpc).

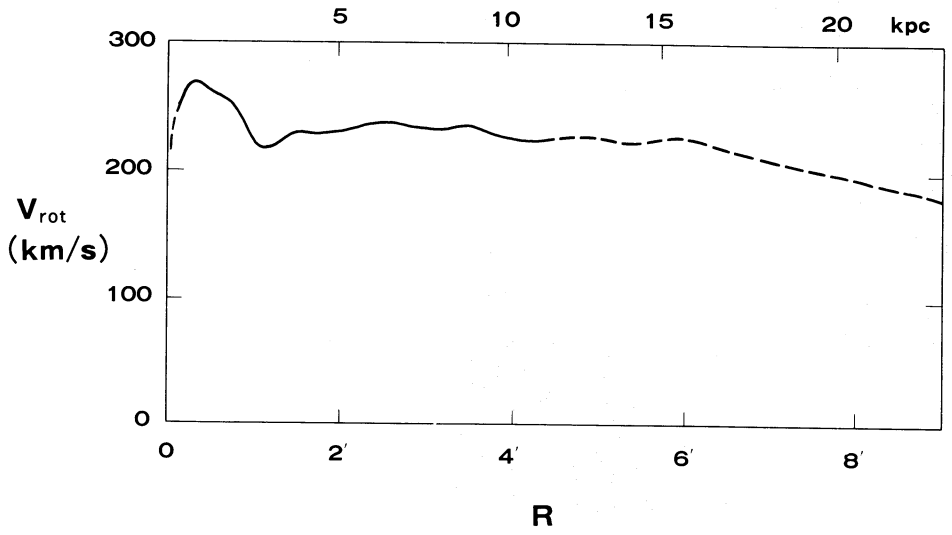

Fig. 6. The CO rotation curve of NGC 891 (full line), combined with the H I rotation curve (dashed line: Sancisi and Allen 1979).

3.8. Disk Thickness: Thin and Extended Molecular Disks

The thick-disk in CO has been extensively discussed by García-Burillo et al. (1992) based on their CO data using the IRAM 30-m telescope. In order to obtain information about the vertical extent of molecular gas above and below the galactic plane, we mapped the $1' < X < 2'$ and $-1' < Y < +1'$ region, which is toward the tangential direction of the 3.5-kpc ring in the northern side. Figure 7 shows a map of the integrated intensity (I_{CO}) for the mapped region; figure 8 shows the intensity cross section perpendicular to the disk, as obtained from figure 7 by averaging from $X = 1'$ to $2'$. The cross section comprises two components; a narrow component with a sharp peak at the disk plane, and a broad component forming an extended outskirt. This result is in a good coincidence with that obtained by García-Burillo et al. (1992).

The half-intensity full width of the narrow component (thin disk) was measured to be 16.″7, slightly larger than the antenna HPBW, 15″. However, if we take into account the pointing accuracy of the observations (±3″) and the grid spacing (15″), we may conclude that the disk is not significantly extended, compared to the HPBW. The upper limit to the intrinsic thickness of this thin disk can be estimated to be about $\sqrt{16.7^2 - 15^2} = 7'' \simeq$ 300 pc, consistent with a thickness of 7″, as obtained from interferometric observations with a resolution of 4.″5 (Handa et al. 1992). From this upper-limit we can derive an upper limit to the tilt angle of the galaxy plane from the line of sight: If we assume a thickness of 100 pc for the molecular disk and a line-of-sight depth of the disk to be about 6 kpc, an apparent thickness of about 300 pc is obtained for a tilt angle of 1.°7. Hence, either the galaxy's molecular disk is not tilted by more than this angle, or the inclination is greater than 88.°3.

The half-intensity width of the broad component (thick, extended disk) is as large as 50″, significantly greater than the beam width, and the intrinsic half-intensity full width is estimated to be $\sqrt{50^2 - 15^2} = 48'' = 2.1$ kpc. This is direct evidence for the existence of an extended molecular gas disk outside the normal molecular disk: This thick disk extends to a height of about ±1 kpc from the galactic plane. This extended molecular gas disk is consistent with the significant optical extinction observed in the halo region of NGC 891 (Aoki et al. 1991), and may be related to a numerous dark lanes in NGC 891, which run perpendicular to the disk and extend for a kpc or more (Sawa and Fujimoto 1987). Similar out-of-disk dust features have been found in many other galaxies (Sofue 1987).

The total CO luminosity involved within the mapped area ($1' < X < 2'$ and $-1' < Y < 1'$) was estimated to be 1.80×10^8 K km s^{-1} pc^2, which corresponds to a molecular mass of $1.05 \times 10^8 M_\odot$. After separation of the components, the thin disk in this area was shown to have a luminosity of 9.3×10^7 K km s^{-1} pc^2 ($1.1 \times 10^9 M_\odot$); the remaining 9×10^7 K km s^{-1} pc^2 ($6 \times 10^8 M_\odot$) is taken by an extended disk. This fact indicates that a significant amount of molecular gas (50% of the entire molecuar gas) exists in the form of the extended disk of 2 kpc thickness.

A beam-corrected thickness of 27″ (= 1.2 kpc) has been obtained for the H I disk (Sancisi and Allen 1979), which is between the widths of the narrow and broad components of the molecular disk. However, since the

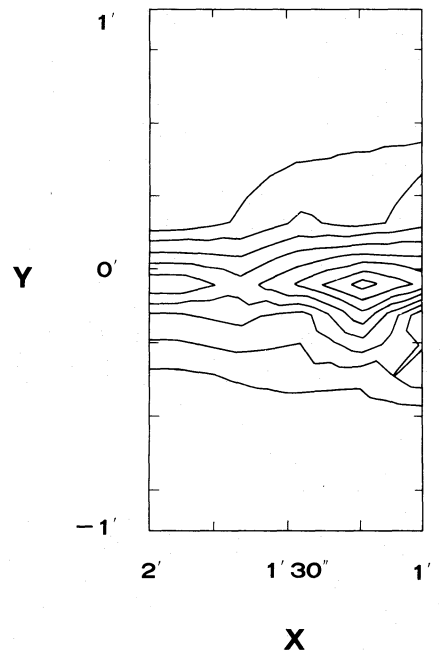

Fig. 7. I_{CO} map toward the tangential direction of the 3.5-kpc ring in the eastern half at $X = 1'$–$2'$. Contours are drawn at 10, 20, 30, ..., 80 K km s^{-1}.

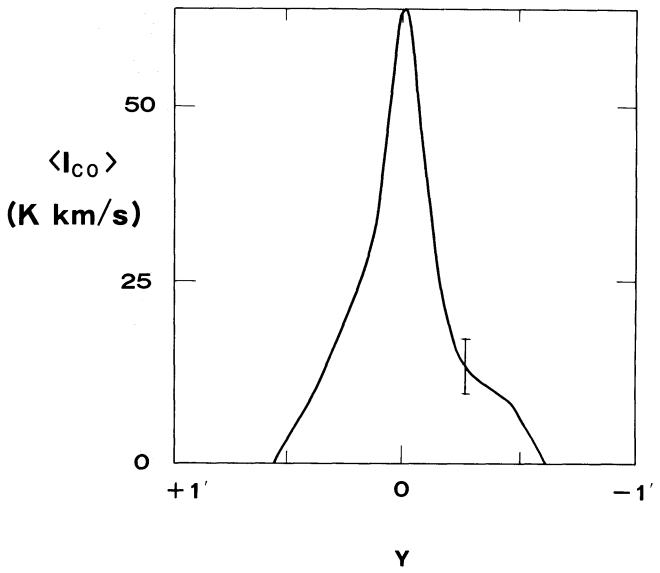

Fig. 8. A cross section of the intensity perpendicular to the molecular gas disk, averaged for the region from $X = 1'$ to $2'$. The vertical bar indicates the typical rms error.

H I observations had a wider beam of 30″ and no separation of components has been applied, we cannot compare our result with the H I result. In addition to these general distributions, a spur feature is visible in figure 7 at $X = 1'.2$ and $Y \sim -15''$; its apparent extent is about 500 pc from the disk plane. The spur is in positional coincidence with the northen CO intensity peak in figure 3a and the radio continuum peak at 6 cm. However, no optical counterpart, such as a vertical dust lane, can be seen in optical photographs (e.g., Sandage 1961).

4. Discussion

In the present ^{12}CO(J = 1–0) observations we obtained almost complete survey data along the major axis of the edge-on galaxy NGC 891 at a resolution of 15″ (654 pc for a 9 Mpc distance). We derived the intensity distribution along the major axis, the total molecular mass, the rotation curve, and an intensity map around an NE section toward the 3.5-kpc ring. We may thus discuss implications of the observed results related to galactic structure and star formation.

4.1. Barred Spiral Galaxy?

It has been argued that a molecular ring with a radius of a few kpc is characteristic for barred spiral galaxies (Nakai 1992) and that the bar length is of the order of the ring radius. In this context the molecular 3.5-kpc ring of NGC 891, clearly seen both in the total intensity distribution in figure 3a and in the density distribution in figure 3c, may indicate that the galaxy has a bar structure of 3.5 kpc length. We also found that the gas at $R < 3$ kpc within the ring is rotating without obeying the usual flat rotation, but is rotating rigidly.

We point out a kinematical relationship of the 3.5-kpc ring to the rotation characteristics: The 3.5-kpc ring, showing the CO peaks at $|X| \simeq 1'.3$, appears at radii where the rotation curve turns from the outer flat part to the inner rigid part (figure 5). It is known that the bar part of SB galaxies generally shows rigid rotation, while normal spirals have flat rotation, even toward the inner region. Therefore, the rotation characteristics of NGC 891 are more like those of a barred spiral. If this is the case, the ring concentration of gas at $R = 3.5$ kpc can reasonably be explained by a sweeping up of gas toward the cusp region between the bar (with a rigid rotation) and outer disk (with a flat rotation). In fact, a numerical simulation has shown that viscous molecular clouds are accumulated at a radius where the rotation characteristcs change from rigid to flat (e.g., Fukunaga 1983). We further comment that the high-density concentration of molecular gas near to the nucleus may be due to accretion caused by this bar structure.

NGC 891 has a box- or peanut-shaped bulge (de Vaucouleurs 1974; van der Kruit and Searle 1981), and an inner Lindblad resonance of a stellar bar is sug-

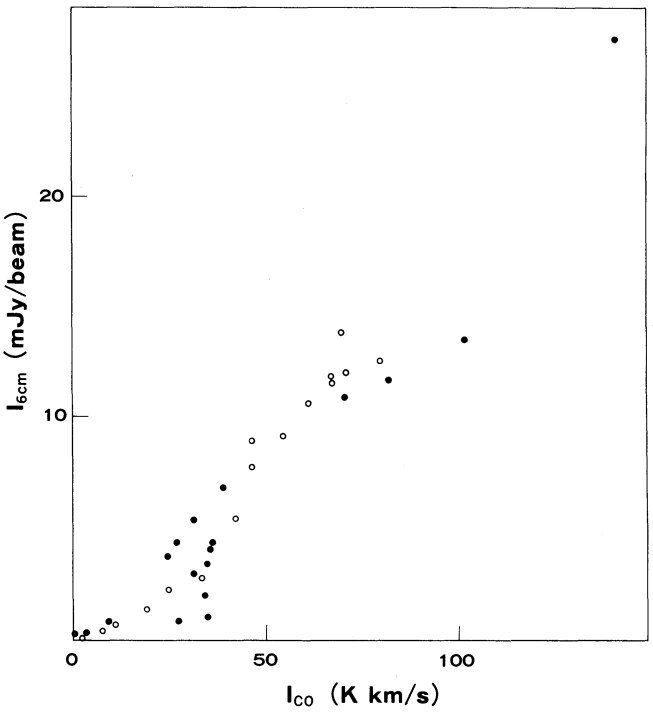

Fig. 9. The 6-cm continuum emission intensity I_{6cm} plotted against the CO intensity, I_{CO}. Open circles are for the NE part, and the filled circles for the SW.

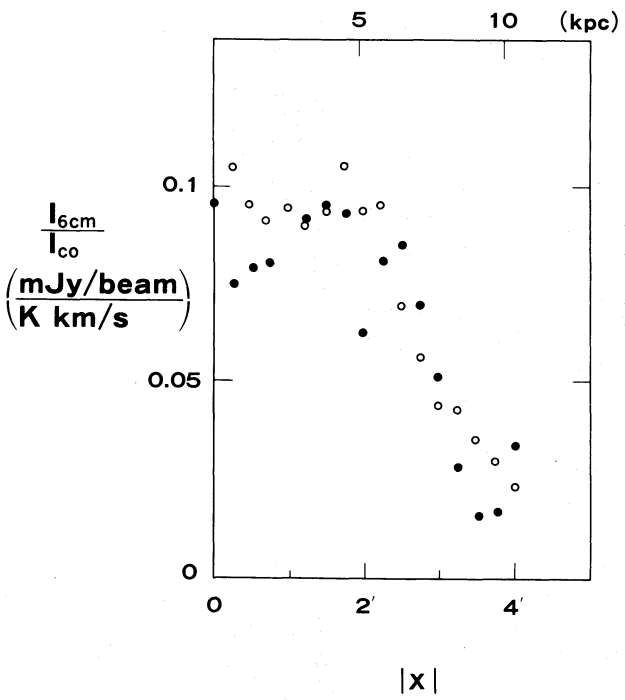

Fig. 10. SFE (star formation efficiency as defined by the ratio of 6-cm radio intensity to the CO intensity) plotted against the distance from the nucleus. Open circles are for the NE half, and filled circles for the SW.

gested as being a possible mechanism for such a shape (Combes and Sanders 1981; Combes et al. 1990). These arguments are all favorable for the assumption that NGC 891 has a bar; we can thus conclude that NGC 891 can better be classified as an SBb than a normal Sb galaxy.

4.2. Threshold Radius for Star Formation

An important aspect of the molecular gas distribution is its relation to star-formation activity. The star-formation rate can be indicated by far infrared emission, while there has been no FIR observations with sufficient resolution. Here, we use 6-cm radio data and discuss the star-formation efficiency. The 6-cm radio continuum emission is a mixture of thermal and non-thermal emission from star forming regions and supernovae-related cosmic rays and magnetic fields. Since their separation is beyond the scope of this paper, we consider here the total 6-cm emission to be a "modified star-formation rate," namely a mixture of thermal activity from H II regions and SN related nonthermal activity (or the mixture of OB star birth rate and SN rate). As discussed in section 3.3, the 6-cm and 21-cm distributions are significantly different from each other (Sukumar and Allen 1991): The 21-cm emission is far more extended than 6-cm, and the 6-cm emission is more correlated with the molecular gas disk. This is reasonably explained by the fact that the 21-cm emission is dominated by nonthermal emission related to the disk-and-halo magnetic fields as well as to widely spread cosmic rays, while the 6-cm emission is predominantly thermal and is more deeply coupled with star-forming activity whithin the gas disk.

In figure 9, we plot the 6-cm intensity against the CO intensity, where each point represents the intensities which were read at every 15″ interval along the major axis from figure 1a of Sukumar and Allen (1991) and from figure 3a of this paper, respectively. [Note that the effective resolution of the present CO observations is 21″ if we take into account the grid spacing of 15″; this is about the same as the HPBW, 20″, of the 6-cm observations by Sukumar and Allen (1991).] In general, we find a good linear correlation between the radio and CO intensities. However, we notice that the radio intensity seems to become weak when the CO intensity decreases to below 30 K km s^{-1}; little radio emission is seen for $I_{CO} < 20$ K km s^{-1}. This may indicate the presence of some threshold in the CO intensity for star-formation to take place; this is most likely related to the position in the galactic plane.

Figure 10 is a plot of a "radio (modified) star-formation

efficiency" (SFE) against the distance from the nucleus along the major axis. Here, SFE is defined by the ratio of the 6-cm intensity to the CO intensity, SFE $= I_{6\mathrm{cm}}/I_{\mathrm{CO}}$ [in units of (mJy/20″ 6-cm beam)/(K km s^{-1})]. SFE is almost constant in the inner region, a sudden decrease is found at $|X| = 2'.2$ (5.7 kpc), beyond which it decreases steeply until $|X| \sim 4'$. We note that the primary beam for the 6-cm VLA observations had an HPBW of $9'$, larger than the size of the concerned region ($8'$); further, the primary beam attenuation was corrected in the used data (Sukumar and Allen 1991). Moreover, except for a few points near to $|X| \sim 4'$, the 6-cm intensities plotted here are greater than 500 μJy/beam, sufficiently greater than the rms noise (25 μJy/beam) of the used map. Hence, the decreasing SFE is real and quite significant, at least up to $X = \pm 3'.5$. We comment that, even if we take into account the H I gas (Sancisi and Allen 1979) and analyze the SFE using the total H I + H_2 gas, we obtain a similar result, an even steeper decreasing SFE beyond $X = \pm 2'$.

From these facts we conclude that there exists a "threshold radius" in the star forming disk, $R_{\mathrm{SF}} = 2'.2 =$ 5.7 kpc. At $r < R_{\mathrm{SF}}$ the star-formation efficiency is almost constant, and is not particularly dependent on the gas density inside this radius. (Note that a constant SFE implies an SF rate increasing with the gas density.) However, the SFE suddenly starts to decrease steeply and monotonically beyond this radius, $r > R_{\mathrm{SF}}$.

We stress that the concept of a threshold radius for the SF disk introduces a new aspect to the star-formation mechanism and chemical evolution in a galaxy: The presence of the threshold radius implies that the star formation is not uniquely determined by the gas density, but is strongly dependent on structural, as well as dynamical conditions within a single galaxy. This could lead one to consider that the time scale for the chemical evolution is dependent on the dynamical situation: The denser and more massive is the stellar disk, the more rapid is the evolution.

Since the gas density in the outer disk decreases with radius, this threshold radius could be related to the concept of the threshold gas density for star formation (Kennicutt 1988), although we cannot distinguish exactly whether the threshold happens depending on the location (radius) or on the density. In either way, it is interesting to estimate the gas density corresponding to the radius. The CO intensity at the threshold radius is about I_{CO} ($X = R_{\mathrm{SF}}$) $\simeq$ 30 K km s^{-1}, or $N_{\mathrm{H_2}}(X = R_{\mathrm{SF}}) \simeq 1.1 \times 10^{22}$ $\mathrm{H_2}$ cm^{-2}. If we take a line-of-sight depth of about 10 kpc toward $|X| = 2'.2$, this value gives a threshold face-on column density of 4.3 $M_\odot$ pc^{-2}. For an assumed disk thickness of 100 pc, this corresponds to a density of 2.26 $\mathrm{H_2}$ cm^{-3}. The H I gas has an integrated intensity of $\sim 5 \times 10^3$ K km s^{-1} ($= 9.2 \times 10^{21}$ H cm^{-2}) at $X = 2'.2$ (Sansici and Allen 1979; Rupen 1990). This gives a surface mass density 1.8 $M_\odot$ pc^{-2}. Hence, the surface mass density of the H_2+H gas is approximately 6.1 $M_\odot$ pc^{-2}. This value agrees with the threshold values obtained by Kennicutt (1988).

4.3. Nuclear Activity and the Molecular Gas Concentration

Finally we mention the relationship between the molecular gas concentration and the nuclear activity in NGC 891.

The 6-cm radio continuum distribution within $r < 2'.2$ (5.7 kpc) coincides exactly with that of CO emission at the present angular resolution (20″) (figures 3a and b). As readily shown in figure 10, the ratio of the radio continuum intensity to the CO intensity toward the center is about the same as that in the disk region at $r <$ 5–6 kpc. A similar correlation is found between the 21-cm (1412 MHz) continuum emission (Sancisi and Allen 1979) and CO, although the 21-cm observations had a lower resolution of 30″ and no detailed comparison can be made. We note that the 21-cm continuum is dominated by non-thermal emission, and is more related to high-energy activity than star formation such as starburst, particularly in the central region.

These facts indicate that the nuclear activity, as long as it is measured by the radio continuum emission, seems to be controlled by the molecular gas density. In other words, we may state that the molecular gas accretion almost directly triggers the nuclear activity of the galaxy.

We thank the staff members at NRO and T. Handa for their help in the observations. This work was financially supported by the Ministry of Education, Science and Culture under Grant No. 01420001 and 01302009 (Y. Sofue).

References

Allen, R. J., Baldwin, J. E., and Sancisi, R. 1978, *Astron. Astrophys.*, **62**, 397.

Aoki, T. E., Hiromoto, N., Takami, H., and Okamura, S. 1991, *Publ. Astron. Soc. Japan*, **43**, 755.

Bloemen, J. B. G. M., Strong, A. W., Blitz, L., Cohen, R. S., Dame, T. M., Grabelsky, D. A., Hermsen, W., Lebrun, F., Mayer-Hasselwander, H. A., and Thaddeus, P. 1985, *Astron. Astrophys.*, **154**, 25.

Combes, F., Debbasch, F., Friedli, D., and Pfenniger, D. 1990, *Astron. Astrophys.*, **233**, 82.

Combes, F., and Sanders, R. H. 1981, *Astron. Astrophys.*, **96**, 164.

Dame, T. M., Ungerechts, H., Cohen, R. S., de Geus, E. J., Grenier, I. A., May, J., Murphy, D. C., Nyman, L.-Å., and Thaddeus, P. 1987, *Astrophys. J.*, **322**, 706.

de Vaucouleurs, G. 1974, in *The Formation and Dynamics of Galaxies, IAU Symp. No. 58*, ed. J. R. Shakeshaft (D. Reidel Publishing Company, Dordrecht), p. 335.
Dickey, J., and Kazes, I. 1992, *Astrophys. J.*, **393**, 530.
Fukunaga, M. 1983, *Publ. Astron. Soc. Japan*, **35**, 173.
García-Burillo, S., Guélin, M., Cernicharo, J., and Dahlem, M. 1992, *Astron. Astrophys.*, **266**, 21.
Handa, T., Sofue, Y., Ikeuchi, S., Kawabe, R., and Ishizuki, S. 1992, *Publ. Astron. Soc. Japan*, **44**, L227.
Huchtmeier, W. K., and Richter, O.-G. 1989, *A General Catalog of H I Observations of Galaxies* (Springer-Verlag, Heidelberg), Table 1.
Kennicutt, R. C. 1988, *Astrophys. J.*, **334**, 685.
Nakai, N. 1992, *Publ. Astron. Soc. Japan*, **44**, L27.
Rupen, M. P., 1991, *Astron. J.*, **102**, 48.
Sancisi, R., and Allen, R. J. 1979, *Astron. Astrophys.*, **74**, 73.
Sandage, A. R. 1961, *The Hubble Atlas of Galaxies* (Carnegie Institution, Washington, D. C.), p. 25
Sanders, D. B., Solomon, P. M., and Scoville, N. Z. 1984, *Astrophys. J.*, **276**, 182.
Sawa, T., and Fujimoto, M. 1987, in *Magnetic Fields and Extragalactic Objects*, ed. E. Asséo and D. Grésillon, Edition de Physique (BP 112, 91944 Les Ulis Cedex, France), p. 165.
Sofue, Y. 1987, *Publ. Astron. Soc. Japan*, **39**, 547.
Sofue, Y. 1992, *Publ. Astron. Soc. Japan*, **44**, L231.
Sofue, Y., Handa, T., and Nakai, N. 1989, *Publ. Astron. Soc. Japan*, **41**, 937 (Paper II).
Sofue, Y., Nakai, N., and Handa, T. 1987, *Publ. Astron. Soc. Japan*, **39**, 47 (Paper I).
Solomon, P. M. 1983, in *Internal Kinematics and Dynamics of Galaxies, IAU Symp. No. 100*, ed. E. Athanasoula (D. Reidel Publishing Company, Dordrecht), p. 35.
Sukumar, S., and Allen, R. J. 1991, *Astrophys. J.*, **382**, 100.
Tully, R. B., and Fisher, J. R. 1977, *Astron. Astrophys.*, **54**, 661.
van der Kruit, P. C., and Searle, L. 1981, *Astron. Astrophys.*, **95**, 116.